

Finite Element Analysis of Experimentally Tested Concrete Slabs Subjected to Airblast

A.S. Augusto^{1,*}, F.B. Mendonça[§], G. Urgessa[#], and K. Iha[@]

¹Defense and Sensitive Technologies Division, Aeronautics and Space Institute, S.J. Campos, SP- 12228-904, Brazil

[§]Research and Development Division, Institute of Operational Applications, S.J. Campos, SP -12228-970, Brazil

[#]Civil, Environmental, and Infrastructure Engineering, George Mason University, Virginia - 22030, USA

[@]Department of Chemistry, Aeronautics Institute of Technology, S.J. Campos, SP -12228-900, Brazil

*E-mail: anselmoaugusto@hotmail.com

ABSTRACT

Since the last century, concrete has been used to protect structures against intentional or accidental detonation of explosives. Recently, as concerns about terrorist activities and accidents in plants using explosives increase worldwide, the study of the behaviour of this type of material and any civil or military structure under the influence of explosions has increased. Among the lethal effects of explosive devices, which cause greater loads in structural elements is the airblast effect. For this reason, this paper presents a series of airblast finite element (FEM) simulations developed in Abaqus/Explicit®. To validate the computational method, such simulations are geometrically and structurally kept similar to full-scale tests conducted in a blast test area of the Science and Technology Aerospace Department (Brazilian Air Force). Both simulations and tests consisted of seven reinforced concrete slabs with compressive strengths of about 40 to 60 MPa, variable steel reinforcement areas, slab dimensions measuring 1×1 m, and subjected to 2.7 kg of non-confined plastic bonded explosive. The results demonstrated that FEM simulations can predict the rupture of the tested slabs and how the effect occurs, showing a valid method to investigating the response of RC slabs when compared to expensive field tests. Differences in displacements were observed between the results of FEM simulations and blast field tests, mainly caused by the sensitivity of the case studied, limits of computational capacity, and intrinsic variations in the materials and sensors used in the field tests. However, these differences showed an order of magnitude compatible with the safety coefficients used with RC, demonstrating that the method can be used for the design of RC slabs under the effect of airblast.

Keywords: Blast effect; Reinforced concrete; Finite element analysis; FEM; Dynamic analysis

NOMENCLATURE

A, B, C, n, m	FEM model constants
D	Variable that measures damage in FEM, where value 0 means intact material and 1 means ruptured material
D_1 and D_2	FEM model damage constants
E	Elasticity Modulus in GPa
E_{ci}	Initial tangent elasticity modulus of concrete in GPa
E_{cs}	Secant modulus of elasticity of concrete in GPa
f_c	Compressive strengths of concrete in MPa at 28 days
G	Shear modulus of elasticity in GPa
P	Hydrostatic tensile stress or concrete tensile stress in MPa
P^*	Dimensionless hydrostatic tensile stress or concrete tensile stress
R	Standoff distance in m
T	Maximum hydrostatic tensile stress or concrete maximum tensile stress in MPa
T^*	Dimensionless maximum hydrostatic tensile stress or concrete maximum tensile stress
W	TNT equivalent mass in kg

ε	Equivalent plastic strain
μ	Volumetric strain
ρ	Density in $\text{kg} \cdot \text{m}^{-3}$
ρ_0	Initial density in $\text{kg} \cdot \text{m}^{-3}$
σ	Stress in MPa
σ^*	Dimensionless equivalent stress
$\dot{\varepsilon}$	Strain rate
$\dot{\varepsilon}^*$	Dimensionless equivalent strain rate equal to $\dot{\varepsilon}/\dot{\varepsilon}_0$
$\dot{\varepsilon}_0$	Dimensionless equivalent strain in s^{-1}

1. INTRODUCTION

Among the possible targets that may be impacted by the effects of explosions, civil and military buildings stand out. Such buildings are subjected to blast due to military actions, terrorist acts, or accidental explosions. The blast effect, in addition to generating serious economic losses, will result in human and material losses^{1,2}. This makes it important to study these effects on buildings under two types of analysis: in the design of explosion-resistant installations or, in military actions, in the selection of the most suitable armament to neutralise a military target¹.

An explosion is a sudden release of energy and gases at high pressure and temperature, which causes several effects, most of which are lethal^{3,4}. This release compresses the

surrounding fluid, generating a mechanical shock wave that moves in all directions with an epicenter at the origin of the detonation^{3,5}. This effect is called airblast and is characterised by high pressure and supersonic displacement. Airblast generates loads in buildings that exceed the dimensioned capacity, as they are commonly lateral and with pressure peaks much higher than usual, causing severe damage or total ruin¹. Among the types of existing structures, this paper highlights reinforced concrete (RC), because it is the most ideal to support and protect buildings from airblast waves⁶.

Due to these factors, explosives and the airblast effect on concrete targets raised worldwide attention and motivated a series of studies and publications in the area⁷⁻⁹. Among the studies published to predict airblast effects, this article highlights those that use the Finite Element Method (FEM) and full-scale tests. The article by Ngo⁸, *et al.* studied the response of a structure under the airblast effect, presenting FEM simulations developed in LS-Dyna[®]. Nalagotla¹⁰ compared the results of LS-Dyna[®] with SDOF (Single-Degree-of-Freedom System) methods for an RC slab. Vannucci¹¹, *et al.* showed the values of reflected pressure of a shock wave on plane bulkheads obtained with empirical equations or FEM simulations with Autodyn[®]. Casagrande¹² used LS-Dyna[®] to determine the impulsive loads from explosions. Mendonça¹³⁻¹⁸, *et al.* presented the result of a set of full-scale tests of explosions on RC slabs.

Among the articles that used Abaqus/Explicit^{®19}, Mokhtari and Nia^{20,21} presented TNT detonation simulations in buried metal tubes. Mougeotte²², *et al.* compared the overpressure results obtained in the FEM simulation with the predicted empirical values. Jablonski²³, *et al.* presented a computer simulation accompanied by a series of full-scale experiments, both representing the detonation of a land mine under a vehicle. Melo²⁴ shows FEM simulations developed in Abaqus/Explicit[®] of the impact of metallic casing armaments on RC slabs and validates the method with experiments.

This current paper is a continuation of Mendonça¹³⁻¹⁸, *et al.*, developing a series of FEM computer simulations of the airblast effect originating from the detonation of Plastic Bonded Explosives (PBX) on RC slabs and comparing the results with the tests presented by Mendonça¹³⁻¹⁸, *et al.* One of the main contributions of the paper is to validate the Abaqus/Explicit[®] program¹⁹ in simulations of airblast effects on RC using JH2²⁵ and HJC²⁶ constitutive models, previously used in the literature only for simulations of metallic projectiles on RC slabs^{24,28,29}. Another unique aspect of this paper is the validation of the FEM models with full-scale explosive tests.

2. MATERIAL AND METHODS

2.1 Constitutive models

The constitutive models of the materials used in the FEM simulation are presented below.

2.1.1 Johnson-Cook Model

In 1983, after a series of tests on ductile materials at various temperatures, with high torsions and strain rates, Johnson and Cook²⁷ presented a constitutive model for metals. Such a model is suitable for situations where a metallic material undergoes large deformations at high speed, such as those occurring in

explosions. Eqn (1) presents the von-Mises stress (σ_v) used in the model, which takes into account the strain rate²⁷. The effect of temperature in reducing the strength of the metal was neglected.

$$\sigma_v = (A + B\varepsilon^n)(1 + C \ln \dot{\varepsilon}^*) \quad (1)$$

2.1.2 JH2 Model

Johnson and Holmquist developed the JH2 model²⁵ in 1994 to simulate brittle rupture materials under the effect of large deformations, high strain rates, and high pressures, such as concrete parts under impacts or explosions. In this model, unlike stress-strain curves, equations of state depending on material strength, pressure, strain, strain rate, and the variable D that measures the progression of damage to the material are formulated. This damage variable is accumulated over the integration cycles, culminating in the failure of the material, when D reaches²⁴ the value 1.

The stresses (σ) in this model are normalised by the equivalent stress in Hugoniot Elastic Limit (σ_{HEL}) and the hydrostatic stresses by the pressure component at HEL (P_{HEL}), according to Eqns (2) and (3)^{24,25}. The value of the equivalent stress σ_{HEL} is calculated according to Eqn (4).

$$\sigma^* = \sigma / \sigma_{HEL} \quad (2)$$

$$P^* = P / P_{HEL} \quad (3)$$

$$\sigma_{HEL} = \frac{3}{2}(HEL - P_{HEL}) \quad (4)$$

where HEL is Hugoniot's one-dimensional elastic limit.

The dimensionless equivalent stress in the material is calculated according to Eqn (5), where the stress between the intact material and the material under failure is weighted, using the damage variable. These stresses are calculated, respectively, using Eqns (6) and (7)^{24,25}.

$$\sigma^* = \sigma_i^* - D(\sigma_i^* - \sigma_f^*) \quad (5)$$

$$\sigma_i^* = A(P^* + T^*)^n (1 + C \ln \dot{\varepsilon}^*) \quad (6)$$

$$\sigma_f^* = B(P^*)^m (1 + C \ln \dot{\varepsilon}^*) \quad (7)$$

where σ_i^* and σ_f^* are the dimensionless stresses of the intact and failure material.

D is calculated according to Eqn (8), while the equivalent plastic failure strain (ε_{fp}) is obtained from Eqn (9)^{24,25}.

$$D = \sum \frac{\Delta \varepsilon_p}{\varepsilon_{fp}} \quad (8)$$

$$\varepsilon_{fp} = D_1(P^* + T^*)^{D_2} \quad (9)$$

where $\Delta \varepsilon_p$ is the plastic strain accumulated in each integration cycle.

Hydrostatic pressure (P) is also calculated using equations of state, its value for intact material being a polynomial function dependent on volumetric strain, according to Eqns (10) and (11)^{24,25}.

$$P = K_1\mu + K_2\mu^2 + K_3\mu^3 \quad (10)$$

$$\mu = \rho/\rho_0 - 1 \quad (11)$$

where K_1 is the bulk modulus of the material and K_2 and K_3 are constants.

For tensile stresses, the pressure value is modified to $P = K_1\mu$. When the material begins to suffer damage, that is, D becomes greater than 0, there is an increase in pressure called ΔP , according to Eqn (12). This increment is calculated for each integration cycle using an energy method, presented in Eqn (13)^{24,25}.

$$P = K_1\mu + K_2\mu^2 + K_3\mu^3 + \Delta P \quad (12)$$

$$\Delta P = -K_1\mu_{t+\Delta t} + \sqrt{(K_1\mu_{t+\Delta t} + \Delta P_{t+\Delta t})^2 + 2\beta K_1\Delta U} \quad (13)$$

where β is a constant, determined experimentally, that represents the fraction of the internal energy loss converted into potential hydrostatic energy. ΔU is the energy loss in an increase of integration time, determined in Eqn (14). The value of U is calculated according to Eqn (15) and represents the internal energy of the shear and deviatoric stresses^{24,25}.

$$\Delta U = U_{D(t)} - U_{D(t+\Delta t)} \quad (14)$$

$$U = \frac{(\sigma_{HEL}\sigma^*)^2}{6G} \quad (15)$$

2.1.3 HJC Model

The material constitutive model of Holmquist, Johnson, and Cook²⁶ was presented in 1993 and is widely used in simulations of impact on concrete slabs^{24,28,29}. This model is very similar to JH2 and was developed specifically for concrete under the effect of large deformations at high speed. The first difference is in the calculation of the dimensionless equivalent tension, which follows Eqn (16). The values are normalised according to the compressive strength of the concrete (f_c), as described in Eqns (17) and (18).

$$\sigma^* = \sigma/f_c = [A(1-D) + B(P^*)^n] [1 + C \ln \dot{\epsilon}^*] \leq S_{\max} \quad (16)$$

where S_{\max} is the maximum dimensionless equivalent tension.

$$P^* = P/f_c \quad (17)$$

$$T^* = T/f_c \quad (18)$$

Another difference is in D , which considers the volumetric plastic strain (μ_p), in addition to the equivalent plastic strain component for failure (ϵ_{fp}), according to Eqn (19)^{24,26}. These components are calculated similarly to the JH2 model, as shown in Eqn (20), being limited inferiorly by $\epsilon_{f,\min}$, to limit the plastic strain of the fractured material^{26,28}.

$$D = \sum \frac{\Delta\epsilon_p + \Delta\mu_p}{\epsilon_{fp} + \mu_p} \quad (19)$$

$$\epsilon_{fp} + \mu_p = D_1(P^* + T^*)^{D_2} \geq \epsilon_{f,\min} \quad (20)$$

However, the main difference is in the pressure state equation as a function of the volumetric strain, which is divided into three regions: one elastic, one transition, and the last with totally dense concrete.

Unfortunately, the Abaqus/Explicit[®] software has not implemented the HJC model in its routines. Because of this, following the already validated work by Melo²⁴, the HJC model will be adapted to JH2. The first solution is the adoption of n equal to 0, so that Eqn (16) becomes similar to Eqns (5) to (7). The second solution is to adopt $\sigma_{HEL} = P_{HEL} = f_c$ so that the normalisations are coherent between the models. Thus, through Eqn (4), the HEL value is equal to $5f_c/3$. Adopting these hypotheses, the only differences are summarised in the P's equations of state and the fact that the HJC model considers the term of volumetric plastic strain (μ_p) in D .

2.1.4 Formulation for Wood

In the full-scale blast test, the concrete slabs were supported by wood frames. It is complex to characterise, obtain parameters, and elaborate numerical simulations for structural members of wood. Considering this, and remembering that such material was used only as a support for the test slabs, it was decided to adopt a simplified but coherent model. The wood was assumed to be a perfectly elastic material, without damage and orthotropic, with three axes of analysis, related to the growth of the wood fibers, called longitudinal, radial, and tangential. The stiffness matrix used for the wood and the stress-strain ratio is presented in Eqn (21)³⁰⁻³².

$$[\sigma] = [C][\epsilon] \Rightarrow \begin{bmatrix} \sigma_{ll} \\ \sigma_{rr} \\ \sigma_{tt} \\ \sigma_{lr} \\ \sigma_{lt} \\ \sigma_{rt} \end{bmatrix} = \begin{bmatrix} C_{ll} & C_{lr} & C_{lt} & 0 & 0 & 0 \\ C_{lr} & C_{rr} & C_{rt} & 0 & 0 & 0 \\ C_{lt} & C_{rt} & C_{tt} & 0 & 0 & 0 \\ 0 & 0 & 0 & G_{lr} & 0 & 0 \\ 0 & 0 & 0 & 0 & G_{lt} & 0 \\ 0 & 0 & 0 & 0 & 0 & G_{rt} \end{bmatrix} \begin{bmatrix} \epsilon_{ll} \\ \epsilon_{rr} \\ \epsilon_{tt} \\ \epsilon_{lr} \\ \epsilon_{lt} \\ \epsilon_{rt} \end{bmatrix} \quad (21)$$

where $[\sigma]$ is the stress vector, $[C]$ the stiffness/elasticity matrix of the wood, $[\epsilon]$ the strain vector, C_{xy} the component in the xy direction of the elasticity matrix, G_{xy} the modulus of elasticity in the plane shear xy , and l, r and t the subscripts for the longitudinal, radial and transversal direction of the wood.

2.2 Full-scale Tests

For the development of the simulations of this work, a model case was studied based on full-scale tests already performed¹⁸, to validate the FEM method. Such tests consisted of detonating cylindrical PBX charges above a slab supported by wooden easels, as shown in Fig. 1. To verify the response of the slab in different situations, the detonation distance, the strength of the concrete, and the reinforcement ratios were varied in a sequence of 7 tests. Some output parameters were measured, but the most important for this paper is the maximum slab displacement over time.

The simulations carried out in the present work tried to reproduce, to the maximum, the conditions of the tests, taking into account all the dimensional variables and mechanical characteristics of the elements. The support that held the explosive in its original position was disregarded in the FEM simulation, as it did not interfere with the displacement of the shock wave to the slab. Likewise, the soil was considered a rigid surface. The slabs measured 1,000 x 1,000 mm and were

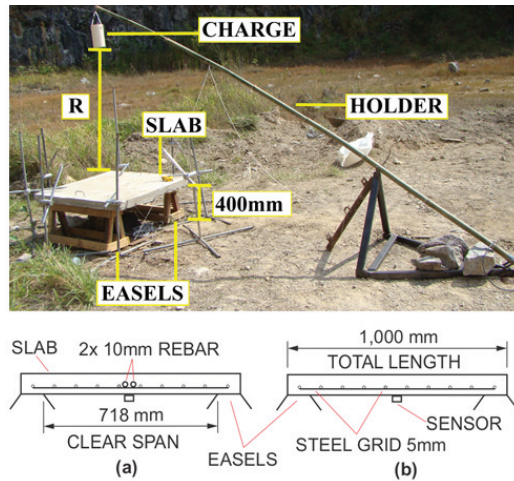


Figure 1. Test Setup with the cross-section of the slab: (a) two-way 5mm steel grid with additional two 10 mm rebar in one-way and (b) tow-way only ¹⁸.

reinforced with a 5 mm steel grid with 100 mm or 150 mm spacing. Some slabs received extra steel reinforcement, with two 10 mm rebar, spaced 100 mm apart. The steel used in the reinforcement was Brazilian grade CA-50 with 500 MPa of yield strength. All the slabs were simply supported on two wooden easels, which rested on the ground. The explosives were cylindrical and had a diameter of 100 mm, the height of 200 mm, were initiated on their upper face, and had a mass of TNT equivalent from 2.50 kg to 2.70 kg. The distance from the slab to the ground was 400 mm and the one direction clear span was 718 mm.

Working of displacement sensor was a wire emanating from potentiometers that were attached to the bottom surface of the slabs and recorded their upward and downward movement during the blast action. The potentiometer sensors, with a sampling rate of 0.42 ms and sensitivity of 1.1×10^{-6} m, were protected against surrounding debris in a steel box under the setup.

Table 1 summarises all tests simulated in the present work. The cylindrical TNT equivalent (W_{cil}), the original of the tests, was converted into spherical TNT equivalent (W_{esf}) to make possible the use of the CONWEP[®] plug-in, which considers all-spherical charges. This conversion has proceeded as described by Esparza³³.

Table 1. Summary of the characteristics of the tests and simulations performed¹⁸

Test	f_c	Rebar 5 mm area	Rebar 10 mm area	W_{cil}	W_{esf}	R
	(MPa)	(cm ²)	(cm ²)	(kg)	(kg)	(m)
Slab 1	42.1	1.3744	0.0000	2.76	10.04	1.3
Slab 2	53.0	1.3744	1.5708	2.72	7.00	2.0
Slab 3	62.0	1.9635	0.0000	2.69	6.90	2.0
Slab 4	53.0	1.3744	1.5708	2.58	6.55	2.0
Slab 5	62.0	1.9635	0.0000	2.60	6.61	2.0
Slab 6	62.0	1.9635	0.0000	2.72	7.00	2.0
Slab 7	42.1	1.3744	0.0000	2.60	7.89	1.6

The purpose of the variation of the input parameters is to observe the behaviour of the slab in the tests and FEM simulations in different airblast conditions. Slab 1 and 7 had the most severe conditions, with smaller distances to explosive charges. The other slabs had a bigger distance of 2.0 m and nearby mechanical characteristics; therefore it was expected that these slabs had similar and less intense results.

2.3 FEM simulation

2.3.1 Modelling

The concrete was modelled as a C3D8R hexahedral solid Lagrangian element with a mixed JH2 and HJC constitutive model. The values of compressive strengths of concrete (f_c) were obtained by tests of rupture of collected specimens, presented by Mendonça¹⁸. The tensile strength (T) and shear modulus of elasticity (G) were calculated as a function of f_c , as recommended by the ABNT 6118 standard³⁴. Other concrete parameters were obtained in the literature^{24,28,29,35}, according to Table 2. The use of some coefficients as constants, as bulk modulus K_1 , for different strength concretes was adopted for other validated and published works^{24,29}. Such hypotheses did not affect the results of the FEM simulations presented by their authors, obtaining results very similar to those observed in field tests.

Table 2. Variable (a) and constant (b) parameters used for concrete in the simulation^{24,28,29,34,35}

Parameters that vary with the concrete's strength (a)			Constant parameters (b)				
f_c (MPa)	42.10	53.00	62.00	K_1 (GPa)	85.00	C	0.01
E_{ci} (GPa)	36.34	40.77	41.99	K_2 (GPa)	-171.00	$\dot{\epsilon}_0$	1.00
E_{cs} (GPa)	32.89	38.02	40.10	K_3 (GPa)	208.00	S_{max}	7.00
G (GPa)	13.71	15.84	16.71	A	0.79	β	1.00
T (MPa)	3.63	4.23	4.36	n	0.00	D_1	0.04
HEL (MPa)	70.17	88.33	103.33	B	1.60	D_2	1.00
P_{HEL} (MPa)	42.10	53.00	62.00	m	0.61	$\epsilon_{f,min}$	1.00
				ρ (kg/m ³)	2440	$\epsilon_{f,max}$	0.01

The reinforcing rebar was inserted as one-dimensional B31 Lagrangian elements and modelled following Johnson Cook's equations. They were fixed to the concrete using the EMBEDDED ELEMENT command. In such a tool, the nodes of the embedded beam elements are perfectly joined to the nodes of the external solid element²⁴. The adoption of an embedded beam in FEM simulation had three main reasons: it was the solution taken for all references that considered the rebar in concrete^{10,24,35}; the use of beams instead of C3D8R elements significantly reduces computational effort and optimise meshing; the field tests showed that did not occur any kind of slip between rebars and concrete.

The definition of steel parameters was based on the work of Rajput³⁵, *et al.* who considered Weldox[®] 460E steel, presented by Børvik³⁶, *et al.*, as the concrete reinforcement. Such steel has a yield stress of 490 MPa, very similar to those

used in the present work. The considered steel parameters for Johnson Cook's equations are shown in Table 3.

Table 3. Parameters used for reinforcement in the simulation^{35,36}

ρ (kg/m ³)	7850	E (GPa)	200
		ν	0.33
A (MPa)	490	n	0.73
B (MPa)	807	m	0.94
C	0.0114	$\dot{\epsilon}_0$ (1/s)	5.00E-04

The wooden easels were modelled with C3D8R hexahedral solid Lagrangian elements and 10mm constant mesh. As the easels had a less significant influence on the results, the largest possible mesh was used that could represent the complex shape of such objects, without computationally overloading the model. As previously discussed, wood was considered to be a perfectly elastic orthotropic material, with the stiffness matrix obtained in the work of Gonçalves³⁰, *et al.* The wood used was *Eucalyptus saligna* with a rigidity matrix of Eqn (22). The density considered³⁰ was 850 kg/m³.

$$[C] = \begin{bmatrix} 28.122 & 10.931 & 3.111 & 0 & 0 & 0 \\ 10.931 & 8.633 & 2.171 & 0 & 0 & 0 \\ 3.111 & 2.171 & 3.041 & 0 & 0 & 0 \\ 0 & 0 & 0 & 2.486 & 0 & 0 \\ 0 & 0 & 0 & 0 & 0.851 & 0 \\ 0 & 0 & 0 & 0 & 0 & 0.851 \end{bmatrix} \text{ GPa} \quad (22)$$

The soil was modelled as a rigid and fixed two-dimensional R3D4 shell.

For the calculation of airblast loads impacting concrete, the CONWEP[®] plug-in³⁷ on Abaqus/Explicit[®] was used, as it is a widely validated tool and based on empirical data from the Kingery and Bulmash equations³⁸. Such equations are used by several defense manuals and institutions^{1,2}.

2.3.2 Mesh Refinement

To choose the best mesh for the concrete and steel elements, which are the main materials under the airblast effect, a convergence analysis was carried out. The simulation of slab 2 was used as a model for this investigation, observing the response of the maximum displacement in the center of the slab as a function of the variation in the mesh size. This analysis was performed up to the limit of the available computational resources and was reached when the mesh was a size of 5 mm. The results showed a clear increase in damage and slab displacement as the mesh size decreased, which was expected. The displacements did not converge within the range of analysed meshes, in contrast to the damage, which stabilised from the 6mm mesh. Thus, it was decided to adopt the most refined mesh possible within the available computational limitations, i.e., with 5mm elements.

2.3.3 Simulation Process

The finite element software Abaqus/Explicit^{®19} was used for the development of the FEM simulation for each of the

tests listed in Table 1. The simulations were performed using 4 processors of 3.3 GHz and 8 GB of RAM. In Fig. 2(a), the geometry used in the simulation is shown, presenting a cut in the visualisation of the concrete, so that the reinforcement inserted could be partially revealed. Figure 2(b) shows the details of the mesh, after refinement. This configuration resulted in a simulation with about 650,000 nodes, 579,000 C3D8R hexahedral elements, 10,000 R3D4 shell elements, and from 2,660 to 3,800 B31 beam elements, depending on the reinforcement used. The simulations were extended until the slab reached its first displacement peak or suffer a total rupture, resulting in simulation times of 50 to 300 ms, which were processed from 12 to 80 hours.

3. RESULTS AND DISCUSSION

The comparative results of the FEM simulation and the tests are summarised in Table 4, showing the displacements in the center of the lower face of the slab at the first negative peak and the mean and standard deviation of these values, considering the slabs that did not have a total rupture.

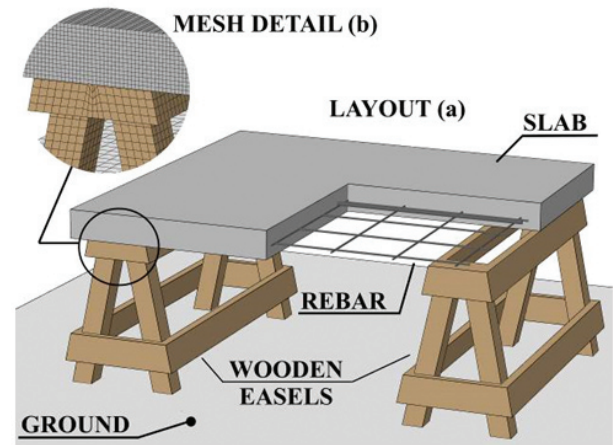


Figure 2. Geometry layout (a) used in FEM program with detail of mesh (b)¹⁹.

Table 4. Comparative results between tests and FEM simulation

Test	Displacement on the first negative peak (mm)		Relative difference from the test
	Test	FEM	
Slab 1	Total rupture in both scenarios		
Slab 2	39.80 ¹	19.06	Outlier ¹
Slab 3	16.92	17.97	+ 06.21 %
Slab 4	24.63	16.19	- 34.27 %
Slab 5	22.29	15.97	- 28.35 %
Slab 6	22.23	19.45	- 12.51 %
Slab 7	Total rupture in both scenarios		
Mean ²	21.52	17.73	- 17.61%
Standard deviation ²	3.26	1.60	- 50.92%

1. The result of Slab 2 in the test was considered an outlier, thus it was not considered in the mean and standard deviation of the test values

2. Mean and standard deviation of displacement from the slabs that did not have a total rupture, disregarding the outliers

The result of Slab 2 in the test was considered an outlier, as the measured displacement was around twice the mean. It was due to a probable failure of the sensors during testing. Both Slab 1 and 7, which were closer to the explosive and had less resistance, showed total rupture, both in tests and in the FEM simulation. In Fig. 3, it was observed the test result for Slab 1, which was similar to Slab 7. Figure 4 shows, for the same slab, the evolution of the damage in the concrete during the simulation with the same full breaking pattern verified in the test. In this figure, the colour of the slab indicates the damage to the material. The redder it is, the closer to the fracture and deletion of the element. Such deletion of the damaged element is an existing feature in the software. The elements indicated in blue do not present any type of damage. The time displacement curve in the center of the bottom of Slab 1 is shown in Fig. 5(a), comparing the FEM method with a traditional theoretical SDOF method that will not be described in the present work and follows the recommended by Cormie and Geoff¹. In the tests of Slabs 1 and 7, the displacement was not measured in the tests, as the sensors were damaged due to



Figure 3. Slab 1 post-test, fractured in a similar way to FEM¹⁸.

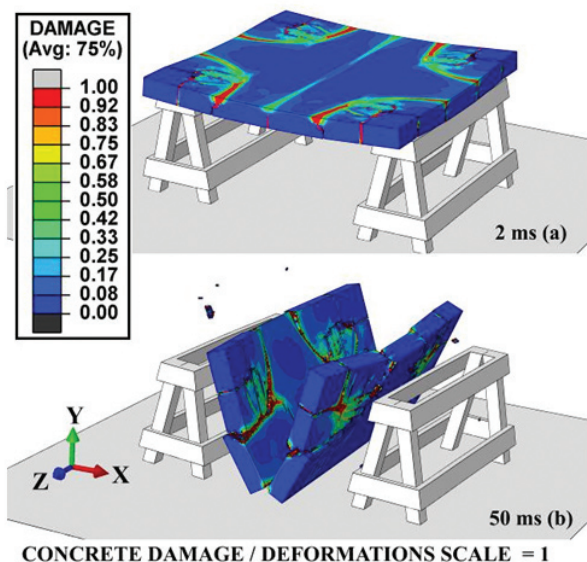


Figure 4. Damage in the concrete obtained with FEM simulation for Slab 1, after 2 ms (a) and 50 ms (b) of detonation¹⁹.

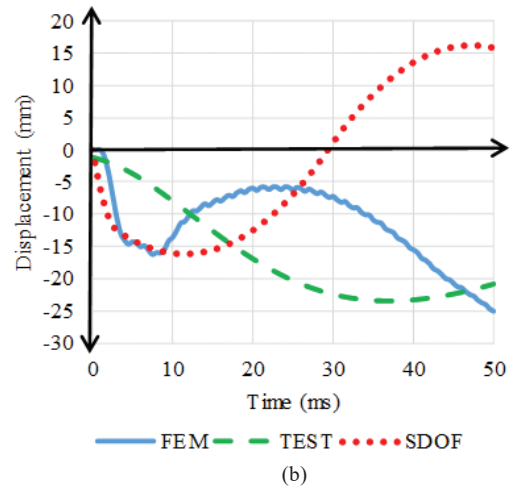
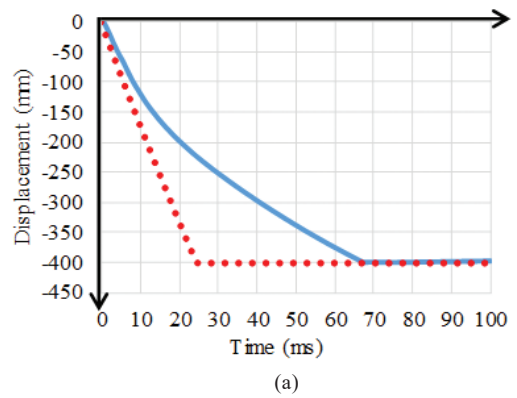


Figure 5. Comparative displacement curves in the center of the slab as a function of the time of Slab 1 (a) and Slab 4(b).

rupture. Finally, the analysis of the FEM data from the rebar showed that the reinforcement of Slabs 1 and 7 suffered plastic strains of up to 60 % and stresses of 1 GPa, which severely exceed the steel limits, representing similarly to what was observed in the experiments.

The other slabs (2 to 6) responded to the airblast in a very similar way, as expected, with small changes only in the magnitude of the displacements. Both in the simulation and the tests, the slabs showed prominent cracks in the concrete faces but did not rupture. As shown in Fig. 6, in both methodologies, there are more pronounced transverse cracks in Slab 4, accompanied by discrete longitudinal cracks. Naturally, the cracks in the tested slab are less symmetrical and have more random tracing, resulting from the irregularity of the real material. Figure 5 (b) shows the comparative displacement curves for Slab 4 in different methods. Lastly, the analysis of the FEM data from the rebar showed that the reinforcement of the slabs 2 to 6 suffered plastic strains of up to 18% and stresses close to steel ultimate tensile strength, not sufficient for a rupture.

The results of the presented FEM simulation demonstrate that the method was effective in predicting the rupture of the tested slabs. When there was no collapse, the numerical simulation showed a pattern of cracks similar to the tests, showing its effectiveness in predicting damages. However, the numerical simulation tended to have lower peak displacements

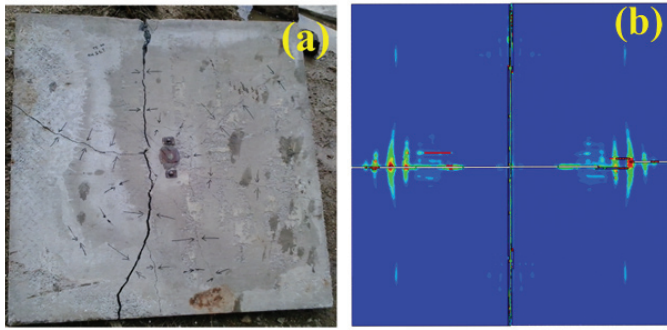


Figure 6. Comparison of damage to the underside of slab 4 during the test (a) and with the use of FEM (b)^{18,19}.

than the tests. This difference was around 18 % in the mean with a maximum of 34 % in Slab 4, disregarding outliers. Such values may look high in a first analysis, but it is usual when working with concrete elements under dynamic loads like an airblast. RC elements are heterogeneous and consist of several materials with variable and unpredictable sizes and sources, such as cement, sand, and stone. Due to this, the safety factors in RC structures are usually higher. As a reference, the Brazilian RC standard³⁴ defines that during the RC designs the loads must be increased by 20 % and the concrete strength must be diminished by 20 % too, considering rare and exceptional conditions. In regular conditions, the standard defines that both coefficients are 40 %. These safety values are usual and similar to other international RC standards. Then, the differences between the FEM and tests have an order of magnitude less than or equal to the safety coefficient usually applied in RC structures.

The variation in the displacement differences between the test and simulations, even within safety limits, were caused for some factors:

- (a) Slabs 2 to 6, even with equal distance to the explosive and nearby mechanical characteristics, have some small differences in the concrete strength, rebar areas, and TNT equivalent;
- (b) Sensitivity of the case studied: During the development of the present work, it was observed, both in the theoretical calculations and in the simulation, that small changes in the input parameters generated significant variations in the displacement at the center of the slab. This can be corroborated by the tests themselves, where very similar slabs had different results due to a small variation in the TNT equivalent. This sensitivity leads to significant variations in the results even with small variations in the input parameters, and;
- (c) Intrinsic variations of the field tests and used materials: there are inaccuracies in the measurements, variations in the assembly of the experiment, ignorance of test parameters, and unpredictable variations in material characteristics that cannot be evaluated and applied in numerical simulations. Bearing in mind that tests were characterised by high speeds and pressures, the measurement and control of each parameter of the problem are not trivial. These small uncertainties, even more so in a sensitive model, lead to variations in experimental results and a greater standard

deviation in the tests compared to the FEM simulations, as observed in Table 4.

FEM simulation results tended to be less conservative. It was expected and was caused by two factors related mainly to the limitation of computational capacity:

- (a) Mesh size: The computational resources available limited the refinement of the mesh used, however, in the convergence test it was observed that there was a tendency for a small increase in displacements with the use of finer meshes;
- (b) Not considering soil deformation in numerical simulation: The soil was simply considered rigid in the simulation.

The first reason for adopting this hypothesis was the lack of accurate data of soil characteristics on the actual blast test site. The second factor was the variation of these characteristics across the test site. Even so, during the development of the simulations, a deformable ground was tested using estimated parameters. However, this option demanded a great computational effort, requiring a coarser mesh that resulted in more inaccurate simulation. The photographic records of the tests show that there was variable sinking of the supporting wooden easels in the ground, in the order of magnitude of millimeter unit. Such sinking was small, and even it contributed to increasing the displacement results in the field tests, their impact does not interfere with the rupture behaviour of the slab, which is the main objective of the simulation.

4. CONCLUSION

This paper presents finite element analysis of experimentally tested concrete slabs subjected to airblast using the Abaqus/Explicit^{®17}. For this, simulated results were compared with a set of full-scale blast tests. The FE analysis was able to predict the collapse mechanism of slabs that failed during the field test and the damage and crack patterns of those slabs that did not collapse in the field. About the displacements measured in the slabs that did not fail, the finite element analysis produced less conservative results than the field tests. However, the differences between the FEM simulations and the tests showed magnitude compatible with the safety coefficients used in RC structure designs. Plausible explanations are provided in the paper including the assumptions used in the modelling. Also, the displacements in the center of the slab proved to be sensitive to the input parameters, thus, even the small method limitations and simplifications lead to greater variation in the results. Overall, the finite element simulations were proven to be a valuable and viable method for investigating the response of RC slabs when compared to expensive field tests.

REFERENCES

1. Cormie, D. & Geoff, M. Blast effects on buildings. Ed. 2. Thomas Telford, London, 2009. 338 p.
2. U.S. Department of Defense. Structures to resist the effects of accidental explosions. UFC 3-340-02, Washington, USA, 2008. https://www.wbdg.org/FFC/DOD/UFC/ARCHIVES/ufc_3_340_02.pdf. [Accessed on 21 February 2020].
3. Goel, M.; Matsagar, V.; Gupta, A. & Marburg, S. An abridged review of blast wave parameters. *Def. Sci. J.*,

- 2012, **62**(5), 300–6.
doi: 10.14429/dsj:62.1149
4. Sharma, P.; Patel, B. & Lal, H. Blast Valve Design and Related Studies : A Review. *Def. Sci. J.*, 2016, **66**(3), 242–50.
doi:10.14429/dsj.66.9618
 5. Anandavalli, N.; Lakshmanan, N.; Iyer, N.; Prakash, A.; Ramanjaneyulu, K.; Rajasankar, J. & Rajagopal, C. Behaviour of a Blast Loaded Laced Reinforced Concrete Structure. *Def. Sci. J.*, 2012, **62**(5), 284–89.
doi:10.14429/dsj.62.820
 6. Dusenberry, D. O. Handbook for blast-resistant design of buildings. Ed. 1. John Wiley e Sons, New Jersey, 2010. 484 p.
 7. Nazarian, A. & Presser, C. Forensic analysis methodology for thermochemical characterization of ANNM and ANFO homemade explosives. *Thermochimica Acta*, 2015, **608**, 65-75.
doi:10.1016/j.tca.2015.04.006
 8. Ngo, T.; Mendis, P.; Gupta, A. & Ramsay, J. Blast Loading and Blast Effects on Structures – An Overview. *Electron. J. Struct. Eng.*, 2007, Special Issue: Loading on Structures. <http://www.ejse.org/Archives/Fulltext/2007/Special/200707.pdf>. [Accessed on 25 February 2020].
 9. Remennikov, A. The state of the art of explosive loads characterization. University of Wollongong Australia, Wollongong, 2016. <https://scholars.uow.edu.au/display/publication21852>. [Accessed on 03 February 2020].
 10. Nalagotla, J. Pressure-impulse diagrams using finite element analysis for reinforced concrete slabs subjected to blast loading. University of Missouri, Kansas City, 2013. (Master Dissertation). <https://pdfs.semanticscholar.org/710d/fd11b7cf78a23407a6ffdcf730299d29da64.pdf>. [Accessed on 01 March 2020].
 11. Vannucci, P.; Masi, F. & Stefanou, I. A study on the simulation of blast actions on a monument structure. HAL, 2017. <https://hal.archives-ouvertes.fr/hal-01447783v3>. [Accessed on 29 February 2020].
 12. Casagrande, A. S. Estudos de cargas impulsivas com ênfase em explosões. Federal University of Rio Grande do Sul, Porto Alegre, Brazil, 2006. (Master Dissertation in Portuguese).
 13. Mendonça, F. B.; Urgessa, G. S. & Rocco, J.A.F.F. Blast Response of 60 MPa Reinforced Concrete Slabs Subjected to Non-Confined Plastic Explosives. *In* Proceedings of the Structures Congress, American Society of Civil Engineers, Denver, CO, April 2017, 15-26.
doi:10.1061/9780784480397.002
 14. Mendonça, F. B.; Urgessa, G.S.; Iha, K.; Rocha, R. & Rocco, J.A.F.F. Comparison of Predicted and Experimental Behavior of RC Slabs Subjected to Blast using SDOF Analysis. *Def. Sci. J.*, 2018, **68**(2), 138-43.
doi:10.14429/dsj.68.11682
 15. Mendonça, F. B.; Gonçalves, R.; Urgessa, G. S.; Iha, K.; Rocha, R.; Domingues, M. & Rocco, J.A.F.F. Emprego de química computacional na verificação e validação da pressão de detonação de explosivo plástico-PBX. *Química Nova*, 2018, **41**(3), 310-14 (Portuguese).
doi: 10.21577/0100-4042.20170169
 16. Mendonça, F. B.; Urgessa, G. S. & Rocco, J.A.F.F. Experimental investigation of 50 MPa reinforced concrete slabs subjected to blast loading. *Ing. Invest.*, 2018, **38**(2), 27-33.
doi: 10.15446/ing.investig.v38n2.65305
 17. Mendonça, F. B.; Urgessa, G. S.; Dutra, R.; Gonçalves, R.; Iha, K. & Rocco, J.A.F.F. EPS foam blast attenuation in full-scale field test of reinforced concrete slabs. *Acta Sci., Technol.*, 2020, **42**(1), e40020.
doi:10.4025/actascitechnol.v42i1.40020
 18. Mendonça, F.B.; Urgessa, G. S.; Augusto, A. S.; & Rocco, J.A.F.F. Experimental Records from Blast Tests of Ten Reinforced Concrete Slabs. *CivilEng*, 2020, **1** (2), 51-74.
doi: 10.3390/civileng1020005
 19. Simulia. Abaqus/Explicit®. Dassault Systèmes, Vélizy-Villacoublay, 2014.
 20. Mokhtari, M. & Nia, A. A. A parametric study on the mechanical performance of buried X65 steel pipelines under subsurface detonation. *Arch. Civ. Mech. Eng.*, 2015, **15**(3), 668-79.
doi:10.1016/j.acme.2014.12.013
 21. Mokhtari, M. & Nia, A. A. The application of CFRP to strengthen buried steel pipelines against subsurface explosion. *Soil Dyn. Earthq. Eng.*, 2016, **87**, 52-62.
doi:10.1016/j.soildyn.2016.04.009
 22. Mougeotte, C.; Carlucci, P.; Recchia, S. & Ji, H. Novel Approach to Conducting Blast Load Analyses Using Abaqus/Explicit-CEL. *In* Proceedings of the 2010 Simulia Customer Conference, Simulia, Providence, Rhode Island, 2010. <https://apps.dtic.mil/dtic/tr/fulltext/u2/a558175.pdf>. [Accessed on 02 February 2020].
 23. Jablonski, J.; Carlucci, P.; Thyagarajan, R.; Nandi, B. & Arata, J. Simulating Underbelly Blast Events using Abaqus/Explicit - CEL. *In* Proceedings of the 2012 SIMULIA Customer Conference, Providence, Rhode Island, 2012. <https://pdfs.semanticscholar.org/c37e/3beda1a600be1178c2e733d0e15ffb992364.pdf>. [Accessed on 30 January 2020].
 24. Melo, T. B. Modelagem Numérica de Impacto em Concreto Armado Utilizando o Método dos Elementos Finitos. Aeronautics Institute of Technology, São José dos Campos, Brazil, 2011. (Master Dissertation in Portuguese).
 25. Johnson, G. & Holmquist, T. An improved computational constitutive model for brittle materials. *In* Proceedings of the AIP Conference Proceedings 309, American Institute of Physics, Melville, NY, 1994.
doi:10.1063/1.46199
 26. Holmquist, T.; Johnson, G. & Cook, W. A computational constitutive model for concrete subjected to large strains, high strain rates, and high pressures. *In* Proceedings of the International Symposium on Ballistics 14, International Ballistics Society, Quebec City, 1993.
 27. Johnson, G. & Cook, W. A constitutive model and data for metals subjected to large strains, high strain rates and high temperatures. *In* Proceedings of the International Symposium on Ballistics 8, International Ballistics

- Society, The Hague, 1983. <https://archive.org/details/AConstitutiveModelAndDataForMetals/mode/2up>. [Accessed on 10 February 2020].
28. Islam, M. J.; Liu, Z. & Swaddiwudhipong, S. Numerical study on concrete penetration/perforation under high velocity impact by ogive-nose steel projectile. *Comput. Concrete*, 2011, **8**(1), 111-23. doi: 10.12989/cac.2011.8.1.111
 29. Polanco-Loria, M.; Hopperstad, O.; Børvik, T. & Berstad, T. Numerical predictions of ballistic limits for concrete slabs using a modified version of the HJC concrete model. *Int. J. Impact Eng.*, 2008, **35**(5), 290-303. doi: 10.1016/j.ijimpeng.2007.03.001
 30. Gonçalves, R.; Trinca, A. & Cerri, D. Comparison of elastic constants of wood determined by ultrasonic wave propagation and static compression testing. *Wood Fiber Sci.*, 2011, **43**(1), 64-75. <https://wfs.swst.org/index.php/wfs/article/view/1247/1247>. [Accessed on 18 February 2020].
 31. Ballarin, A. W. & Nogueira, M. Caracterização elástica da madeira de eucalyptus citriodora. *CERNE*, 2003, **9**(1), 66-80. (Portuguese). <http://cerne.ufla.br/site/index.php/CERNE/article/download/609/517/>. [Accessed on 06 February 2020].
 32. Simulia. Abaqus Theory Manual. Dassault Systèmes, Vélizy-Villacoublay, 2014.
 33. Esparza, E. Spherical Equivalency of Cylindrical Charges in Free-Air. *In Proceedings of the 25th Department of Defense Explosives Safety Seminar, Department of Defense, Anaheim, USA, 1992*. https://www.researchgate.net/publication/235193804_Spherical_Equivalency_of_Cylindrical_Charges_in_Free-Air. [Accessed on 27 February 2020].
 34. Associação Brasileira de Normas Técnicas. Projeto de estruturas de concreto - Procedimento. NBR 6118:2014, Rio de Janeiro, Brazil. ABNT 2014. (Portuguese).
 35. Rajput, A.; Iqbal, M. & Guptab, N. Ballistic performances of concrete targets subjected to long projectile impact. *Thin-Walled Struct.*, 2017, **126**, 171-81. doi:10.1016/j.tws.2017.01.021
 36. Børvik, T.; Hopperstad, O.; Berstad, T. & Langseth, M. (2001). Numerical simulation of plugging failure in ballistic penetration. *Int. J. Solids Struct.*, 2001, **38**, 6241-64. doi:10.1016/S0020-7683(00)00343-7
 37. Hyde, D. W. Conventional weapons effect (CONWEP) - Application of TM5-855-1. Department of the Army, Vicksburg, 1988.
 38. Kingery, C. N. & Bulmash, G. Airblast parameters from TNT spherical air burst and hemispherical surface burst. Army Armament and Development Center, Ballistic Research Laboratory, Technical Report ARBRL TR-02555. 1984.

CONTRIBUTORS

Mr Anselmo da Silva Augusto received his BE (Civil Engineering) from Aeronautics Institute of Technology (ITA), São José dos Campos, Brazil, in 2007, graduated as Aerial Weapons Specialist, in 2016 and MSc from the same Institute, in 2020. He is currently working in the Aerospace Science and Technology Department - Aeronautics and Space Institute, Brazil. His research interest include dynamic behaviour of structures under blast effect, explosives effects and lethality, design of reinforced concrete structures under dynamic or static loads, numerical simulations and aerial weapons in general. He also works as a civil engineer, developing building projects. His contribution to the current study include the elaboration of theoretical formulation, FEM simulation, results analysis and full paper preparation.

Dr Fausto Batista Mendonça received his BE (Civil Engineering) from Rio de Janeiro State University, Rio de Janeiro, Brazil, in 2001, MSc from University of Brasilia, Brazil, in 2012 and PhD from Aeronautics Institute of Technology (ITA), Brazil, in 2017. He is currently working as engineering researcher in Aerospace Science and Technology Department - Institute of Operational Applications, Brazil. His research interests include full-scale tests, dynamic behaviour of reinforced concrete under blast effect, vulnerability of targets and damage effects. His contribution to the current study include setup preparation, field test and full review of paper.

Dr Girum Solomon Urgessa received his BE (Civil Engineering) from Addis Ababa University, Ethiopia, in 2000, MSc from University of New Mexico, Albuquerque, in 2002 and PhD in 2006. He was a research engineer in the Applied Science Division of Weidlinger Associates, and a structural engineer at Dekker/Perich/Sabatini both in Albuquerque, NM. He is currently working as Associate Professor of Civil Engineering and Affiliate Faculty of the C4I & Cyber Center at George Mason University. His research interests include dynamic response of structures subjected to extreme loads (blast and impact), the use of fibre reinforced polymer composites in structural design and retrofit applications, and structural stability of temporary structures. He has contributed in the results analysis and full review of the paper.

Dr Koshun Iha completed his PhD (Analytical Chemistry) from University of São Paulo (USP), São Paulo, Brazil, in 1991. Currently working as Full Professor of Department of Chemistry, ITA, São José dos Campos, Brazil. He has experience with solid and liquid propellant, energetic materials, ablative materials and rocket engine. He was one of the founders of the National Association of Higher Education Teachers, in Campinas, Brazil, in 1981. He has contributed towards the design of test setup, analysis of experimental tests and full review of paper.